The Role of Folding in the Degradation of Ballistic Fibers

Gale A. Holmes, Jae-Hyun Kim, Derek L. Ho, Walter G. McDonough
Polymers Division, National Institute of Standards and Technology, Gaithersburg, Maryland 20899-8541

Research has indicated that the folding of ballistic fibers comprising soft body armor may be a factor in the performance deterioration that has been observed. To quantify the impact of this failure mechanism on body armor performance, an apparatus was designed and built to simulate the folding that may occur in the ballistic fibers while the vest is in use. This device systematically folds woven fabric and yarns of ballistic fibers to enable an assessment of the impact of folding on ballistic fiber properties. After cycling a piece of woven poly(benzoxazole) (PBO) fabric for 80,000 cycles, a 41% reduction in both the ultimate tensile strength and strain to failure of the PBO fibers was observed. These effects were also observable in data obtained from small angle x-ray scattering (SAXS) where the long range order of the fiber structure is changed by the folding process. Preliminary failure analysis using scanning electron microscopy (SEM) on tested fibers also revealed changes in failure morphology. POLYM. COMPOS., 31:879–886, 2010. Published 2010 by the Society of Plastics Engineers†

INTRODUCTION

In recent years, the deterioration of body armor throughout its service life has been the subject of considerable study [1, 2]. It has been suggested that one possible factor in the performance deterioration observed in worn soft body armor may be the folding of the ballistic fibers that comprise the armor. In an attempt to quantify the impact of this mechanism, an apparatus was designed and built to simulate the folding that may occur to the ballistic fibers while the vest is in use. This effort is part of a research program being conducted by the National Institute of Standards and Technology's Office of Law Enforcement Standards (NIST-OLES) under the auspices of the National Institute of Justice (NIJ). One of the goals of this research on ballistic fibers had been the development of a controlled procedure for simulating the folding that occurs in an actual vest during various stages of its proposed lifespan. This type of procedure would then allow ballistic fiber tests to be performed on body armor whose wear and deformation history are known. Such tests on controlled materials should help to establish the link between use and life expectancy of the body armor.

The apparatus described in this report was designed to fold individual yarns and single and multiple layers of woven fabrics of ballistic fibers by using servo-hydraulic testing equipment that is often available in laboratories that perform fatigue testing of materials. Since the concept is new, a major goal was to incorporate sufficient flexibility into the design to allow most of the deformation parameter space that occurs during actual use to be systematically probed, with the end result being an optimized and relevant deformation protocol. Furthermore, the use of off-the-shelf testing equipment, such as the servo-hydraulic testing equipment, should facilitate peer review and use by others.

MOTIVATION: THE SINGLE FOLD TEST

The research of Cunniff and Auerbach [3] based on virgin yarn data has shown that, within the elastic limit, a correlation exists between the ballistic fiber properties and ballistic performance if the ballistic impact on fiber properties is decoupled from the vest construction parameter of areal density (i.e., the unit mass per unit area). That is, the material properties of the fiber are decoupled from the vest construction parameters known to depend on a manufacturer's vest design. From their research, the correlation between ballistic performance and the mechanical properties of the active fiber is quantified by $(U^*)^{1/3}$ of *Eq. 1*. Therefore, $(U^*)^{1/3}$ is a theoretical parameter that estimates the maximum velocity of a bullet that the fibers of a vest can stop and is independent of vest construction. This equation has also been derived theoretically by Phoenix

Correspondence to: Walter G. McDonough; e-mail: walter.mcdonough@nist.gov

Certain commercial materials and equipment are identified in this article to specify adequately the experiment procedure. In no case does such identification imply recommendation by the National Institute of Standards and Technology nor does it imply that the material or equipment identified is necessarily the best available for this purpose.

DOI 10.1002/pc.20870
Published online in Wiley InterScience (www.interscience.wiley.com).

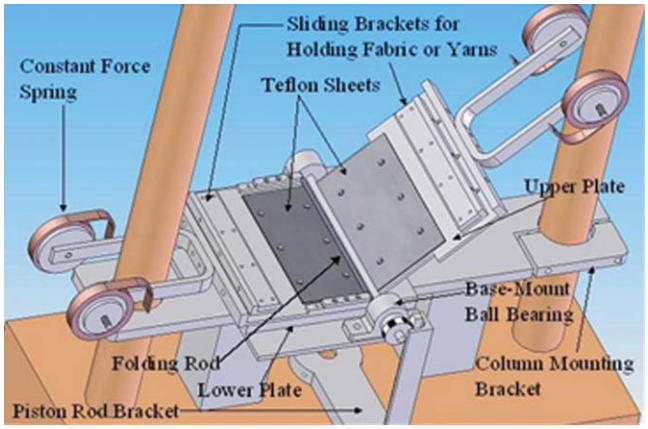

FIG. 1. Basic design of the folding apparatus attached to servo-hydraulic machine. Constant force springs attach to sliding brackets using stainless steel rods (not shown). Note: Delrin brace on piston rod bracket removed to better show clamshell design. [Color figure can be viewed in the online issue, which is available at www.interscience.wiley.com.]

and Porwal [4, 5].

$$[U^*]^{1/3} = \left[\frac{\sigma_f^u \varepsilon_f^u}{2\rho}\sqrt{\frac{E_{1f}}{\rho}}\right]^{1/3} \quad (1)$$

where σ_f^u is the fiber ultimate axial tensile strength (UTS), ε_f^u is the fiber ultimate tensile strain, ρ is the fiber density, and E_{1f} is the longitudinal linear elastic fiber modulus.

In a previous publication, it was shown that a modified single fiber test (m-SFT) [6], based on ASTM C1557-03 [7], could be used to obtain the fiber properties for the above equation. In addition, it was shown that this test could detect changes in mechanical properties, presumably arising from ultraviolet (UV) exposure and hydrolytic action that indicate according to *Eq. 1* [8], a reduction in ballistic performance. Since it is probable that mechanically induced degradation will induce subtle changes in ballistic fiber properties, a preliminary study was conducted where 50 fibers were extracted from a single yarn of virgin poly(benzoxazole) (PBO) fibers and subjected to a single fold. In this report, the visible damage induced by the single fold was accompanied by changes in the fiber properties as measured by the m-SFT [9]. The 10% reduction in strain-to-failure and yield strength observed in the single fold test are significant enough to warrant further study, with the ultimate goal being to link observable reductions in ballistic performance to measurable molecular changes in the ballistic fibers.

It should be noted that another study was performed examining the environmental effects on PBO fibers [10, 11]. The conclusions of this work were that exposure to moisture results in the loosening of the fiber morphology which leads to an increase in the number and size of defects and that the presence of aqueous acid causes both loosening of the fiber structure and hydrolysis of the oxazole ring structure.

EXPERIMENTAL

Folding Apparatus Design and Operation

The design was motivated by the desire to use the controlled fatigue testing features inherent in most servo-hydraulic test machines. To minimize damage to the servo-hydraulic machine by the apparatus, the device was designed to fit on a 250 kN (55 kip) Model 810.25 MTS machine equipped with a 158.5 mm (6.25 in) diameter piston rod. To convert the precise linear motion of the servo-hydraulic machine to precise rotational motion, a bracket was fitted to the piston rod that contained a spur gear and rack [9].

To effect the folding of the ballistic fiber material, a two-piece clamshell design is employed (see Fig. 1). To minimize mass, most of the apparatus is constructed using aluminum, except where otherwise specified. The lower plate is connected to a platform that attached to the servo-hydraulic machine through the column mounting brackets. An interchangeable folding rod with diameter of 6.35 mm was constructed out of stainless steel and attached to this plate. The upper plate is attached to a stainless steel rod that is turned at each end to conform to the required bore size of the spur gear. The top plate is attached to the platform using two base-mount ball bearings that accommodate a shaft.

Each plate is equipped with Teflon sheets to minimize friction between the ballistic material and the plate surface. To hold the fabric or yarn in place, each plate is equipped with a sliding bracket. Each sliding bracket is held in place by two stainless steel rods that attach to constant force springs obtained from Associated Spring Raymond (rods not shown in Fig. 2). These springs maintain constant tension on the woven fabric or yarn.

Modified Single Fiber Fragmentation Test

This test procedure was described in detail in a previous publication [6]. The maximum standard uncertainty in the strain measurements was determined on the 6 cm gauge length specimens to be 0.0001 by performing measurements at 6.1 cm. The standard uncertainty in the load cell at 100 g is 0.001 g.

Small Angle X-Ray Scattering

Small-angle x-ray scattering is a well-known technique to characterize the structure of materials over length scales of sub-nanometers (nm) to 100 nm, depending on the instrumentation. In this work, the SAXS configuration with copper radiation (SAXS-Cu) is in a conventional pinhole (PH) collimation geometry with three pinholes, PH1 = the source pinhole, PH2 = the beam defining pinhole, and PH3 = the sample pinhole, as shown in Fig. 3. The source-to-sample distance (SSD) is fixed at 122.5 cm,

 DOI 10.1002/pc

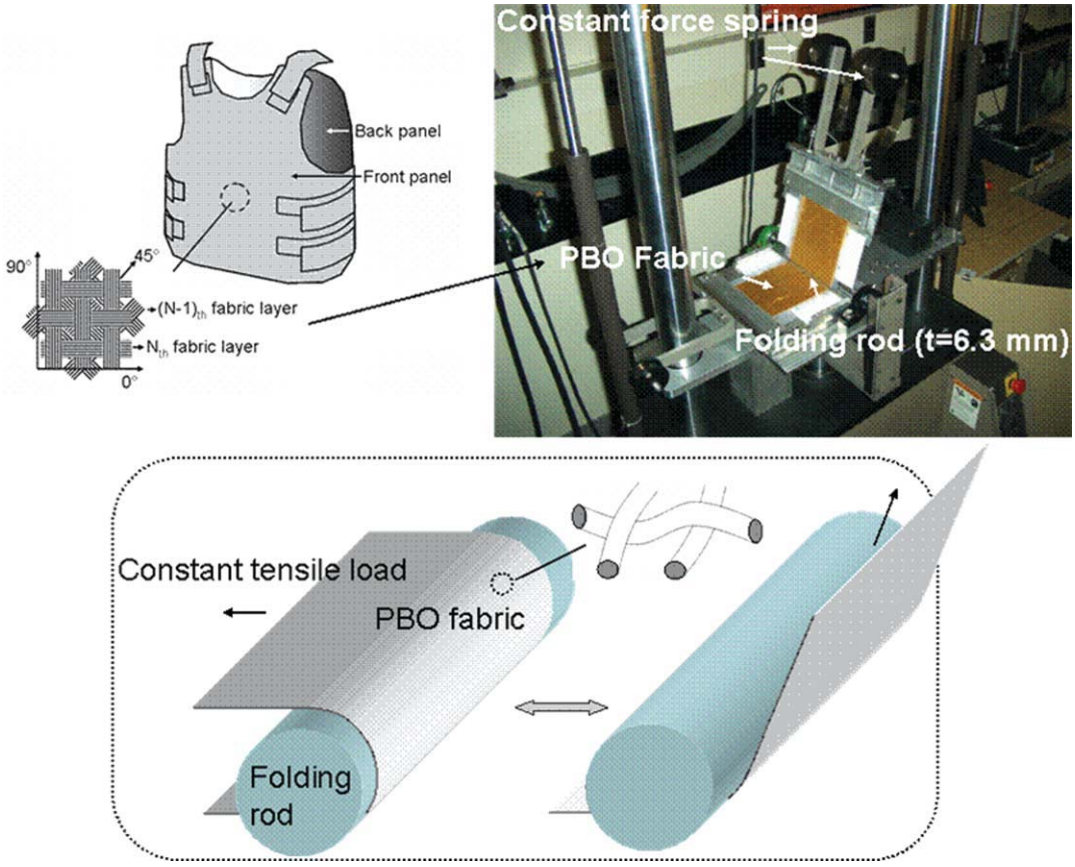

FIG. 2. Schematic of the continuous folding apparatus and folded region. [Color figure can be viewed in the online issue, which is available at www.interscience.wiley.com.]

whereas the sample-to-detector distance (SDD) varies from 26 to 406 cm, yielding an overall wave vector Q [where $Q = (4\pi/\lambda)\sin\theta$, λ is the x-ray wavelength, and 2θ is the scattering angle] range of 0.05 nm^{-1} to 14.90 nm^{-1}, probing a length scale range of about 0.42 nm to 126 nm [12]. $D = 2\pi/Q$ is the corresponding length scale in the real space [13, 14]. The $K\alpha_1$ wavelength of Cu is 0.15406 nm at 8.04 keV. A two-dimensional (2D) 30 cm $\times$ 30 cm image plate is used for the data acquisition [15]. The beam from the source is focused on the detector at SDD = 142 cm (default) through an Osmic multilayer confocal optics.

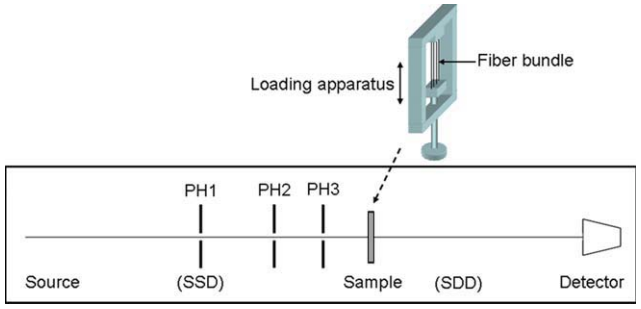

FIG. 3. Schematic shows the pinhole geometry for SAXS-Cu. [Color figure can be viewed in the online issue, which is available at www.interscience.wiley.com.]

In this study, a SAXS-Cu setup with SDD = 406.0 cm for the low-Q scans and 26 cm for the high-Q measurements, the detector pixel size = 200 μm $\times$ 200 μm as well as PH1 = 400 μm, PH2 = 200 μm, and PH3 = 700 μm in diameter, yielding an x-ray beam size of about 300 μm on the sample, was used for the measurements (see Table 1 for more details). The fibers were in a bundle mounted vertically on a sample holder and probed in the transmission mode at room temperature under vacuum.

Scanning Electron Microscopy

A scanning electron microscope was used to investigate changes in surface morphology after cyclic folding and also to characterize the tensile fracture surface of PBO fibers. For investigating the effect of the folding on

TABLE 1. Peak (Q) positions at high Q and the corresponding d-spacing.

Sample	Q_H (nm^{-1})	D_H (nm)	Q_V (nm^{-1})	D_V (nm)
Folded 5.5k	11.55 ± 0.01	0.54	5.37 ± 0.01	1.17
Unfolded 5.5k	11.57 ± 0.01	0.54	5.31 ± 0.01	1.18
Folded 80k	11.65 ± 0.01	0.54	5.37 ± 0.01	1.17
Unfolded 80k	11.61 ± 0.01	0.54	5.34 ± 0.01	1.18

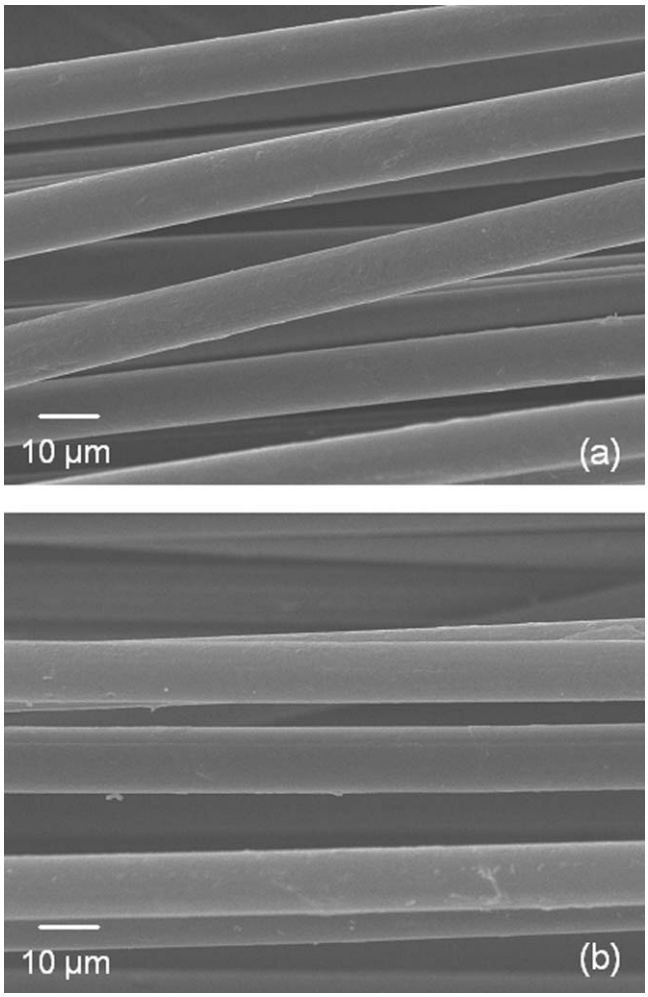

FIG. 4. SEM image of the 5,500 (a) and 80,000 (b) cycle fold PBO fibers.

the PBO fibers, PBO strands were carefully collected from both unfolded and folded fabrics, and these strands were placed on a carbon conductive tape. The fracture mechanisms of PBO fibers after folding and tensile fracture using the m-SFT test were also characterized by placing these specimens on carbon conductive tape. These SEM samples on the carbon tapes were then coated with gold to achieve high resolution images from the SEM.

RESULTS AND DISCUSSIONS

Figure 4 shows an SEM image of PBO fibers after 5,500 (5.5k) and 80,000 (80k) cycles of folding. No damage exists on the surface of the fibers. This suggests that the folding device used in this study generates internal damage and avoids the effect of friction between the folding rod. Figure 5 shows tensile stress–strain behavior of the PBO fibers having the same nominal fiber diameter. Regardless of the cyclic folding, all tested fibers showed non-linear stress–strain behavior until fracture. This unique behavior is a well known property for as-spun PBO fibers. It is known that the degree of the crystallite orientation between core and skin region in the as-spun PBO fiber is significantly different, with the core region with poor chain orientation improving more than that of the skin region under tension. As a consequence, the different stress response of these two regions causes non-linear tensile behavior at the higher strain [16, 17]. Compared to the similarity of the global tensile behavior among the samples, the tensile behavior of the 5.5k folded fibers are more scattered than the other two fibers

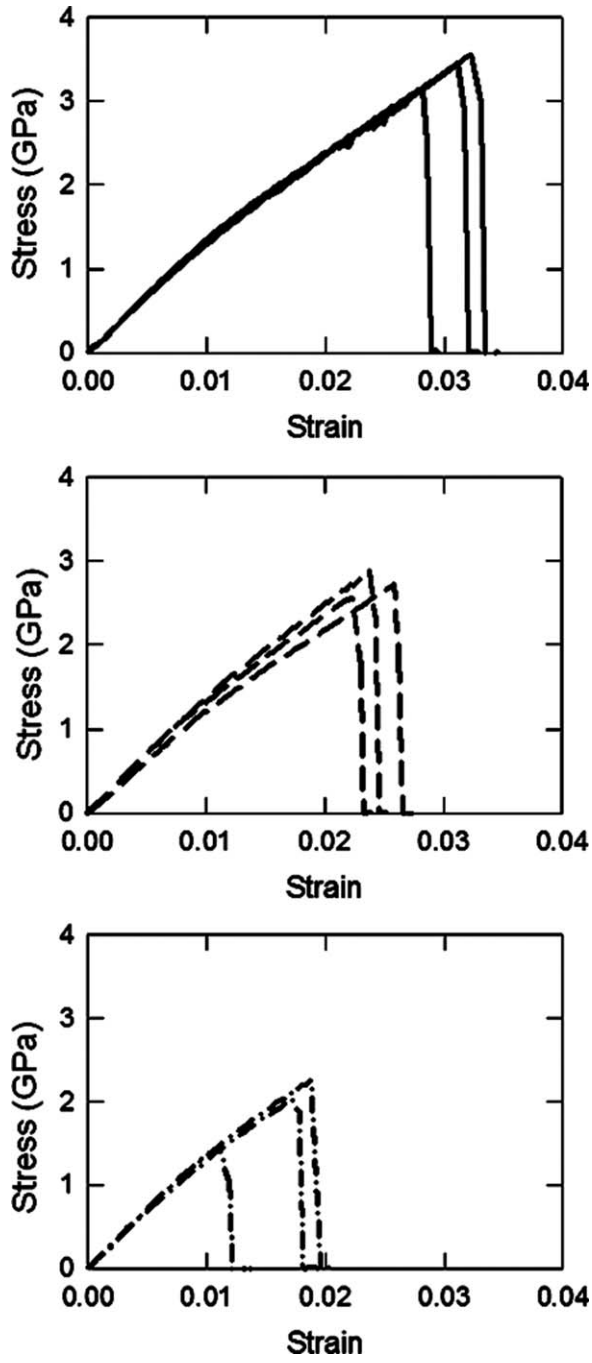

FIG. 5. Tensile stress–strain behavior of the unfolded (—), 5,500 (– –), and 80,000 (– · –) PBO fibers.

DOI 10.1002/pc

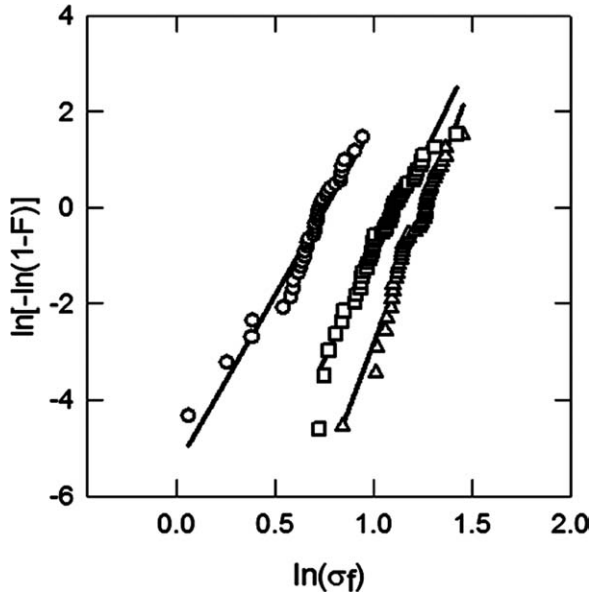

FIG. 6. Weibull plot of the unfolded (Δ), 5,500 (□), and 80,000 (○) PBO fibers.

(i.e., controlled and 80k folded) at the higher strain region. The different tensile behavior of the 5.5k folded fibers implies that a defect size distribution in the fiber is broader than the other two fibers. Therefore, the 5.5k folded fibers are considered to contain the various sizes of defects (i.e., defect size distribution) in each single fiber by folding, while the controlled and 80K folded fibers have no significant size distribution of the flaws in the single fiber. Typically, PBO fibers contain needle like internal voids having approximately 2.4 nm diameters and lengths of 30 nm which are connected each other through cracks or openings between micro fibrils [18]. It is believed that continuous folding can cause a sufficient driving force to nucleate critical defects by growing the cracks between the microfibrils that are perpendicular to the fiber axis and linking the intrinsic microvoids. Eventually, these cracks and microvoids act like intrinsic defects governing the fiber fracture behavior. On the basis of the analysis of the tensile behavior, we can expect that the intrinsic defect size of the controlled fibers is small and the defect size simply grows uniformly to a bigger size when these fibers are folded.

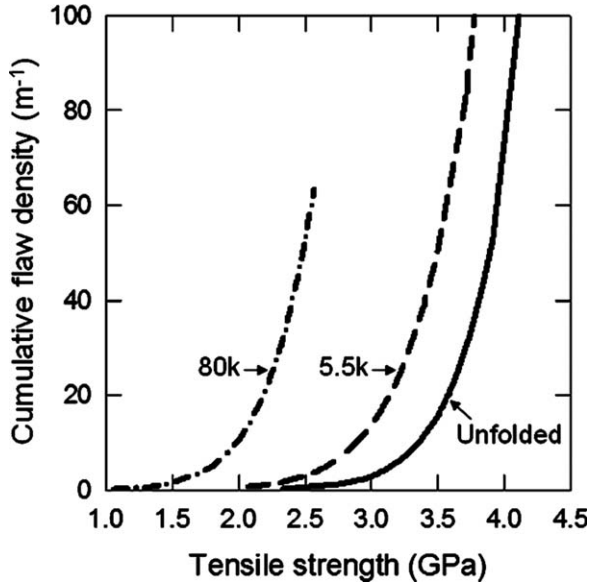

FIG. 7. The relation between flaw density of the unfolded, 5,500, and 80,000 PBO fibers and tensile fracture strength.

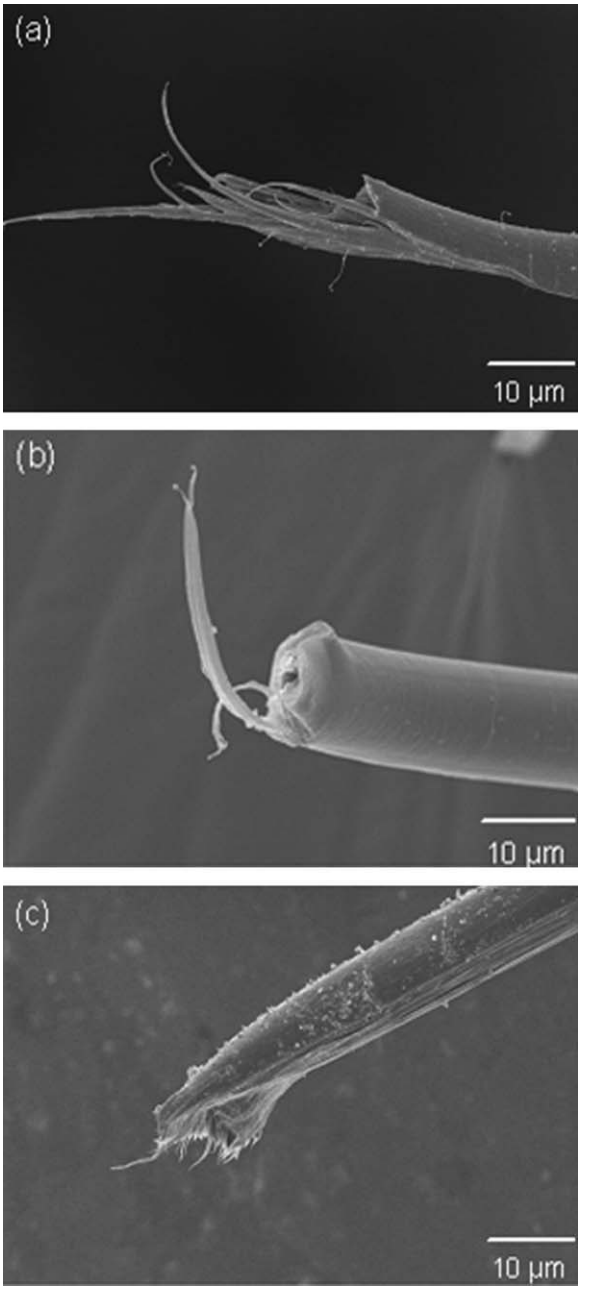

FIG. 8. Fracture surface of the (a) unfolded, (b) 5 500, and (c) 80 000 PBO fibers.

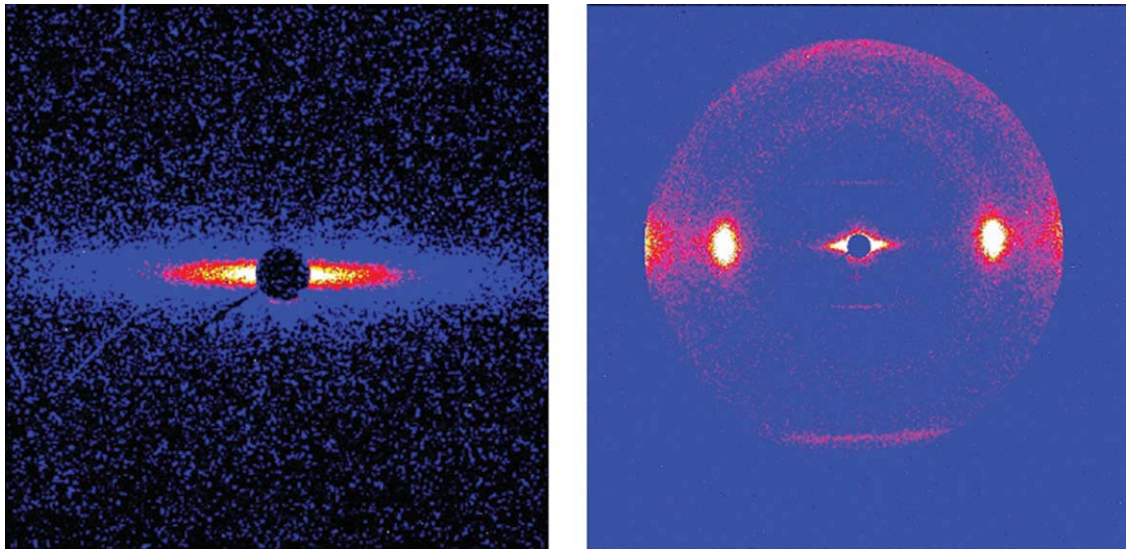

FIG. 9. 2D SAXS-Cu images from the PBO fibers. [Color figure can be viewed in the online issue, which is available at www.interscience.wiley.com.]

Since a fiber fracture mechanism depends not only on defect size but also defect density (i.e., defect number per unit length), we speculated a defect density at a given tensile stress as a function of a degree of the folding. To estimate the distribution of the defects in the fibers, the following analysis was performed [19]. On the basis of the weakest link model, density of defects is an increasing function of stress, since the number of fiber fractures increases with increasing tensile stress. The density of the defects that cause fiber fracture below the stress (σ) is assumed to be given by:

$$\lambda = \frac{1}{L_0}\left(\frac{\sigma}{\gamma}\right)^{\beta} \tag{2}$$

It is further assumed that the strength distribution of a fiber with length (L) can be approximated by the two parameter Weibull distribution

$$F = 1 - \exp\left(-\frac{L}{L_0}\left[\frac{\sigma}{\gamma}\right]^{\beta}\right) \tag{3}$$

where γ is the scale parameter and β is the shape parameter, and L_0 represents for reference length and is chosen to be 1 m. F represents the fracture probability of a fiber in a range of strength from 0 to σ for testing a single fiber. For multiple tests using single fibers, F represents a cumulative distribution of strength that fracture below σ. The Weibull plot with a constant gauge length can be rewritten in *Eq. 3* as the linearized form:

$$y = ax + b \tag{4}$$

where $y = \ln[-\ln(1-F)]$, $a = \beta$, $x = \ln\ \sigma$, and $b = [-\beta\ln\gamma + \ln[L/L_0]]$.

To determine the Weibull shape parameter, the fiber tensile strengths were listed in ascending order and a fiber tensile strength at a rank of an ascending order, σ, was calculated by the following equation:

$$F(\sigma) = \frac{i - 0.5}{N} \tag{5}$$

where i represents an order of a tensile strength in ascending order and N represents the total measured number of the tensile strength. Using the linear least squares method for a fracture probability of the tensile strength, $F(\sigma)$, Weibull plots of the fiber tensile strengths are shown in Fig. 6 and the shape parameter β is 10.91 for the unfolded fibers, 8.41 for the 5.5k, and 7.13 for the 80k fibers. Using the Weibull parameters, the defect distribution in the fibers can be estimated. Figure 7 shows the density of the critical defects calculated by *Eq. 2* as a function of the tensile strength of the non-folded and folded fibers. The densities of the defects of the folded fibers at a given stress level exhibit higher values than the unfolded fibers. This shows that the defects caused by the folding increase in density in the fiber at a given stress, which indicates the higher probability to form critical flaws that are big enough to be able to fracture the fiber as the tensile stress increase. Since these critical flaws under the tensile stress formed by combining the microvoids and cracks in-between along the cross section of the fiber, transverse crack growth is dominant. This speculation agrees well with the fracture surface investigation using SEM in Fig. 8, which show fracture surfaces of the fibers also show transition from longitudinal fiber crack propagation (fibrillation) to transverse crack propagation. Therefore, defects introduced by the cyclic folding appear to be the key parameter that decreases the tensile strength of the fibers. It is known from fundamental studies associated with the yarn test that cracks perpendicular to the fiber axis can be formed by twisting the yarn specimens [20]. On the basis of the analysis of the previous data,

 DOI 10.1002/pc

TABLE 2. Results from the m-SFT tests.

Sample	Diameter (μm)	Modulus (GPa)	Failure strain (%)	Tensile strength (GPa)	Theoretical ballistic performance (m s^{-1})
Virgin fiber (VF)	12.5 ± 0.2	163 ± 10	3.53 ± 0.45	4.46 ± 0.50	802
Single fold VF	12.6 ± 0.3	156 ± 12	3.18 ± 0.50	3.98 ± 0.53	740
Woven fabric	13.1 ± 0.3	143 ± 10	2.97 ± 0.39	3.36 ± 0.57	674
Folded WF (5.5k cycles)	13.0 ± 0.3	146 ± 9	2.50 ± 0.45	2.89 ± 0.42	607
Folded WF (80k cycles)	13.3 ± 0.4	135 ± 8	1.74 ± 0.32	1.99 ± 0.30	472

reduction of the tensile strength is caused by the folding, which, according to Eq. 2, leads to a degradation of ballistic performance of the fibers (Fig. 9).

Finally, it should be noted that the calculation of the critical flaw distribution was obtained by tensile strength data from the single fiber test that is shown in Table 2. For the work presented in this article, 50 fibers were tested and resulted in 40 successful tests (sometimes fiber slippage occurred at the epoxy glue). These tensile strength data of the single fiber test go into λ in *Eq. 2* for the flaw density and the results are shown in Fig. 7. A critical flaw induced by folding can be considered as a function of size or frequency (density). The flaw density was chosen as a metric in this article because information about the flaw size was not obtainable. Figure 7 shows the flaw density level about the stress level which any specimen is likely to fail. For example, an unfolded specimen at a flaw density of 20 per meter fractures at ~3.6 GPa, and an 80k folded specimen at a flaw density of 20 per meter fractures at ~2.2 GPa. Therefore, although the flaw density between an unfolded fiber and a fiber folded 80k times is the same, the fracture stress of an 80k folded fiber is lower than that for an unfolded fiber. This reasoning suggests that the flaw location of 80k agglomerated more closely than the flaw location of the unfolded. Figure 7 shows this relationship among the unfolded, 5.5k and 80k throughout the lowest to highest single fiber tensile strength.

SAXS Study

In addition to the techniques introduced and discussed earlier, the PBO fibers studied were also probed by SAXS-Cu to examine the effect of folding on the fiber structures down to the sub-nanometer level. Figure 9 shows the two-dimensional (2D) raw SAXS-Cu data from one of the fiber samples at both low and high Q. As mentioned earlier in this article, the bundle of fibers was mounted and probed vertically in the x-ray beam, resulting in an anisotropic 2D scattering pattern on the detector along the horizontal axis from the individual crystals aligned within the fibers vertically. The 2D raw data were then averaged both horizontally (H) and vertically (V) within a rectangle of 550 pixels long and 26 pixels wide centered at the beam center and normalized by the corresponding transmission to yield the $I(Q)$ versus Q profile for both low and high Q. $I(Q)$ is the scattered intensity at that specific Q.

SAXS-Cu profiles from the 5.5k and 80k folded/unfolded fiber samples reduced horizontally and vertically are presented in Fig. 10, with an experimental uncertainty less than 1%. Overall, the SAXS-Cu data attest that the folding process has no effects on both the 5.5k and 80k fibers along the vertical fiber orientation/alignment, reflected by the horizontally reduced SAXS profiles, over the Q (length scale) range probed, whereas it slightly affects/changes the structure in the direction perpendicular to the vertical fiber orientation/alignment on a large length scale. A SAXS study where the fiber tension is systematically varied is planned to determine the nature of these observed changes.

CONCLUSIONS

The folding apparatus as designed consistently folded woven fabrics and yarns, and successfully created internal damage in the PBO fibers. Tensile strengths of the folded fibers decreased as the number of cycles increased. The intermediate folding, 5,500 cycle folding, showed 14% reduction and the more rigorous 80,000 cycle folding

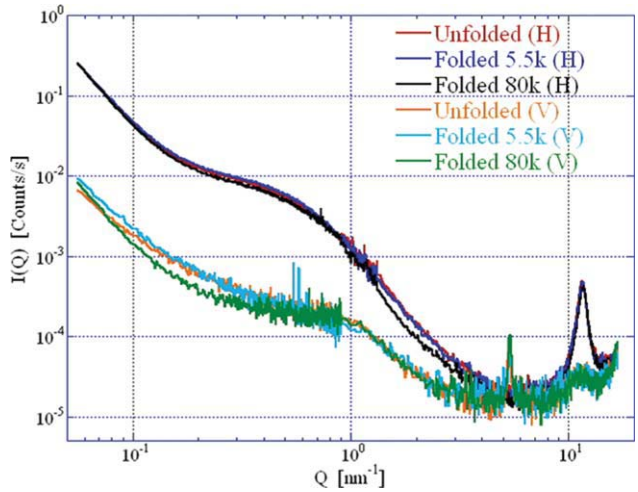

FIG. 10. SAXS-Cu profiles from the PBO fibers. The 2-D raw data were then averaged both horizontally (H) and vertically (V) within a rectangle of 550 pixels long and 26 pixels wide centered at the beam center and normalized by the corresponding transmission to yield the $I(Q)$ versus Q profile for both low and high Q. $I(Q)$ is the scattered intensity at that specific Q. [Color figure can be viewed in the online issue, which is available at www.interscience.wiley.com.]

caused 41% reduction. The degradation mechanism of the tensile strength is believed to be associated with the number of fiber structural flaws that grow to a critical size with increased folding. SAXS analysis, which shows no PBO crystalline damage, also suggests the internal flaw growth through the voids. More testing is planned to determine the optimum and relevant testing conditions required to simulate the impact of mechanical folding over a period of (5–10) years of use. Further tests are underway to quantify the direct mechanism of mechanical degradation.

ACKNOWLEDGMENTS

The authors thank the National Institute of Standards and Technology Office of Law Enforcement and Standards (NIST-OLES) under the auspices of the National Institute of Justice (NIJ) for funding this work. They also thank Dr. W. L. Wu at NIST for valuable discussions contributing to this manuscript.

REFERENCES

1. J. Chin, A. Forster, C. Clerici, L. Sung, M. Oudina, and K. Rice, *Polym. Degrad. Stab.*, **92**, 1234 (2007).
2. G.A. Holmes, K. Rice, and C.R. Snyder, *J. Mater. Sci.*, **41**, 4105 (2006).
3. P.M. Cunniff and M.A. Auerbach, "*23rd Army Science Conference*," Assistant Secretary of the Army (Acquisition, Logistics and Technology), Orlando, Florida (2002).
4. S.L. Phoenix and P.K. Porwal, *Int. J. Solids. Struct*, **40**, 6723 (2003).
5. S.L. Phoenix and P.K. Porwal, *Int. J. Fracture*, **135**, 217 (2005).
6. J.H. Kim, W. McDonough, W. Blair, and G.A. Holmes, *J. Appl. Polym. Sci.*, **108**, 876 (2008).
7. Anonymous. ASTM International, West Conshohocken, PA (2003).
8. G.A. Holmes, K. Rice, and C.R. Snyder, *J. Mater. Sci.*, **41**, 4105 (2006).
9. J.H. Kim, N. Brandenburg, W. McDonough, W. Blair, and G.A. Holmes, *J. Appl. Mech.*, **75**, (2008).
10. P.J. Walsh, X. Hu, P.M. Cunniff, and A.J. Lesser, *J. Appl. Polym. Sci.*, **102**, 3517 (2006).
11. P.J. Walsh, X. Hu, P.M. Cunniff, and A.J. Lesser, *J. Appl. Polym. Sci.*, **102**, 3819 (2006).
12. D.L. Ho, E.K. Lin, C.Q. Wang, R.L. Jones, W.-L. Wu, and G.L. Schmir, A Laboratory Scale Small-Angle X-Ray Scattering Instrument for Critical-Dimension Measurements (2008).
13. J.S. Higgins and H.C. Benoît, *Polymers and Neutron Scattering*, Clarendon press, Oxford, UK (1994).
14. R.-J. Roe, *Methods of X-Ray and Neutron Scattering in Polymer Science*, Oxford, UK (2000).
15. *Rigaku R-Axis IV^{++} CE Marking System (2D Image Plate) Instruction Manual* (Manual Number ME11526A05), (2008).
16. R.J. Davies, M.A. Montes-Moran, C. Riekel, and R.J. Young, *J. Mater. Sci.*, **36**, 3079 (2001).
17. R.J. Davies, M.A. Montes-Moran, C. Riekel, and R.J. Young, *J. Mater. Sci.*, **38**, 2105 (2003).
18. T. Kitagawa, H. Murase, and K. Yabuki, *J. Polym. Sci. Part B: Polym. Phys.*, **36**, 39 (1998).
19. M. Shioya and A. Takaku, *Compos. Sci. Technol.*, **55**, 33 (1995).
20. T. Kitagawa, K. Yabuki, and R.J. Young, *Polymer*, **42**, 2101 (2001).

 DOI 10.1002/pc